An effect of carbonization on the electrorheology of poly(*p*-phenylenediamine)

Tomas Plachy [a,b], Michal Sedlacik [a,c*], Vladimir Pavlinek [a,b], Zuzana Morávková [d], Milena Hajná [d], Jaroslav Stejskal [d]

[a]*Centre of Polymer Systems, University Institute, Tomas Bata University in Zlin, Nad Ovcirnou 3685, 760 01 Zlin, Czech Republic*

[b]*Polymer Centre, Faculty of Technology, Tomas Bata University in Zlin, T. G. Masaryk Sq. 275, 762 72 Zlin, Czech Republic*

[c]*Department of Production Engineering, Faculty of Technology, Tomas Bata University in Zlin, T. G. Masaryk Sq. 275, 762 72 Zlin, Czech Republic*

[d]*Institute of Macromolecular Chemistry, Academy of Sciences of the Czech Republic, Heyrovsky Sq. 2, 162 06 Prague 6, Czech Republic*

ABSTRACT

Particles of poly(*p*-phenylenediamine) were synthesized by the oxidation of *p*-phenylenediamine with ammonium peroxydisulfate at two oxidation levels. They were carbonized at 200 – 800 °C in inert atmosphere and subsequently tested in electrorheological (ER) suspensions. Scanning electron microscopy, Raman spectroscopy and thermogravimetric analysis were used to characterize an influence of the carbonization on the molecular structure and particles size and shape.

* Corresponding author. Tel/Fax: +42 57 603 1444. E-mail address: msedlacik@ft.utb.cz (M. Sedlacik)

Subsequently, ER suspensions were prepared by mixing polymer particles and silicone oil. In order to determine an effect of carbonization on the ER behavior, a number of rheological measurements under various external electric fields were carried out. Dielectric spectroscopy was used for the evaluation of the influence of particles carbonization on the ER performance of suspensions as well. Although the particles carbonized at 600 °C exhibited nearly the same ER effect as the original particles, the efficiency of ER performance was the highest for original, i.e. non-carbonized particles. This is due to lower field-off viscosity in comparison to ER fluids based on carbonized particles.

1 Introduction

Conducting polymers find their use in many applications. Not all of them, however, require high conductivity, and other electrical, optical, or redox properties typical for conducting polymers are exploited. Electrorheology belongs to the group of applications, where the electrical polarizability is a decisive property. An electrorheological (ER) effect is a phenomenon which causes abrupt changes of the viscosity of ER fluids upon the application of an electric field [1, 2]. This reversible change from the liquid to a solid-like state appears in a very short time (within milliseconds) and is accompanied by a distinct transition in rheological properties (viscosity, yield stress or viscoelastic moduli) [3–6]. This performance is highly desired by certain industrial fields, for example, in hydraulic and robotic applications [7]. ER fluids can be used in electrical clutches, torque transducers, dampers, etc. [8]. Nevertheless, there are still some shortcomings that hinder broader utilization of ER fluids in practice [9]. Many materials have been investigated for their ER performance as the dispersed phase with promising results. Unfortunately, they have

not met all requirements on the ER fluids from the application point of view. Hao in his review [5] presents the most important properties that the proper ER fluid should have. Among these, a short response time of the system to the applied electric field, high yield stress, low conductivity, high ER efficiency, low field-off viscosity, and high stability belong [5, 10].

Traditionally, an ER fluid is a two-phase system consisting of insulating carrier liquid and semi-conducting dispersed phase that can be either liquid or solid [5, 11]. At the beginning of the research in the area, many ER systems containing water had been investigated. These suspensions were found unsuitable due to the content of water causing device corrosion. In addition, evaporation can negatively influence the liquid to solid-like state transition in time [12] and ER properties would be lost at elevated temperature. A substantial effort has recently been focused on investigation of polymeric materials for ER systems. Previous investigations have shown the possibility of utilization of conducting polymers as the dispersed phase. In particular, polyaniline (PANI), polypyrrole, poly(*p*-phenylene), poly(acene quionone) radicals, and their derivatives and composites are of concern [1, 11, 13–17]. These polymers display unique properties due to the conjugated system of π-bonds and presence of charge carriers that cause them to be electrically conducting. In other words, this structure enables charge transfer and, consequently, particle polarization in an electric field [5, 12].

It is assumed that the interfacial polarization has a crucial effect on the ER phenomenon [5], thus dielectric and electric properties of particles are the dominant factors determining the intensity of ER effect [9]. The dispersed particles start to be polarized in electric field and their spatial distribution changes from random to highly organized. This transition leads to the creation of particle columns and chains

oriented in the electric field direction. As a result, the system with oriented structure can withstand forces applied while the electric field is on [8, 13].

Conducting polymers exposed to elevated temperature have recently been investigated as a new class of materials applicable in electrorheology [18–20]. They have been modified by heat treatment in air up to 300 °C [18, 20, 21]. This treatment reduces conductivity of these polymers, the property which often causes undesirable current drifts. The exposure to temperatures ≈600 °C in inert atmosphere or in vacuum converts them to nitrogen-containing carbons [19, 22, 23]. Such materials have not been used in electrorheology yet. The fact that the morphology is retained during carbonization belongs among interesting features of this process [22, 24, 25]. So far, attention has especially been paid to various PANI and polypyrrole morphologies. For example, PANI [19, 22, 26–28] or polypyrrole [23] nanotubes/nanofibres were converted to analogous one-dimensional carbons. The ER response of carbonized conducting polymers, however, is still has to be investigated.

The above approach can be extended to other polymers, such as poly(*p*-phenylenediamine). Trlica et al. [14] focused on the ER response of different isomers of polyphenylenediamine, i.e. a PANI derivate, particles in silicone oil. In this case, the best ER performance was achieved for the poly(*p*-phenylendiamine) (P*p*PDA) isomer. Therefore, P*p*PDA particles were chosen as a reference material in the present study, which investigates the influence of various temperatures of P*p*PDA carbonization on its ER response. To evaluate the ER response rheological measurements comprising steady-state shear and oscillatory tests in the absence and in the presence of electric field have been performed. Moreover, thermogravimetric analysis, Raman spectroscopy and scanning electron spectroscopy were used to

follow changes in the structure of carbonized particles. Dielectric properties of the suspensions were also investigated as the interfacial polarization is assumed to be an important factor of the ER performance of ER suspensions.

2 Experimental

2.1 Synthesis of PpPDA

P*p*PDA was prepared by the oxidation of 0.2 M *p*-phenylenediamine (Fluka, Switzerland) with 0.25 M or 0.5 M ammonium peroxydisulfate (APS) (Lach:Ner, Czech Republic) in 0.4 M hydrochloric acid at room temperature. Next day, the precipitated oxidation product was separated by filtration, rinsed with 0.4 M hydrochloric acid, then with acetone, and dried at room temperature.

2.2 Carbonization

Thermogravimetric analysis was used at first as an analytical tool of P*p*PDA carbonization. This was performed in 50 cm^3 min^{-1} nitrogen flow rate at a heating rate of 10 °C min^{-1} with a TGA 7 Thermogravimetric Analyzer (Perkin Elmer, UK). A comparative experiment in air was also done for comparison.

At preparative scale, 5 g portions of the polymer were placed into an electric oven in nitrogen stream and the temperature was increased at 20 °C min^{-1} to the target temperature. Then, the heating was switched off and the sample was left to cool down to room temperature still in nitrogen atmosphere.

2.3 Raman spectroscopy

Raman spectra excited with a HeNe 633 nm laser were collected on an inVia Reflex Raman spectroscope (Renishaw, UK). A research-grade DM LM microscope (Leica, Germany) with an objective magnification ×50 was used to focus the laser

beam on the sample placed on an X–Y motorized sample stage. The scattered light was analyzed by the spectrograph with holographic grating 1800 lines mm^{-1} for HeNe laser. The dispersed light was registered by a Peltier-cooled CCD detector (576×384 pixels).

2.4 Preparation of ER suspensions

The P*p*PDA particles were ground in a ball mill Lab Wizz 320 (Laarmann, The Netherlands), sieved on sieves with pores diameter of 45 μm, and dried in a vacuum oven at 60 °C for 24 h. The suspensions of particles in silicone oil (Lukosiol M200, Chemical Works Kolín, Czech Republic, viscosity η_c = 200 mPa s, conductivity $\sigma_c \approx 10^{-11}$ S cm^{-1}) were prepared in 10 wt% concentration. Before each experiment, the suspension was stirred with a glass stick for ca 5 min and then sonicated for 1 min to insure homogeneous distribution of particles within a suspension.

2.5 Electrorheological measurements

The rheological measurements were carried out using a rotational rheometer Bohlin Gemini (Malvern Instruments, UK) with a plate-plate geometry (a diameter 40 mm with a gap of 0.5 mm between plates) at 25 °C. To determine the rheological parameters of ER fluids, steady-state shear tests were performed. Before each measurement step the suspensions were sheared for 60 s at a shear rate of 20 s^{-1} to destroy residual internal structures.

In order to determine viscoelastic behavior of suspensions, oscillatory tests were performed. Firstly, an amplitude (dynamic strain) sweep test was done to determine the linear viscoelastic region. Consequently, a frequency sweep test with fixed strain (γ = 0.0004 obtained from amplitude sweep test) in this region within 0.1 – 1 Hz was carried out. External electric field strengths within 0.5 – 3 kV mm^{-1} were generated

by a DC high-voltage source TREK 668B (TREK, USA). Prior to shearing the ER fluid in applied field, there was a 60 s delay to provide the particles time to build up the internal structures.

2.6 Dielectric measurements

An impedance analyzer Agilent 4524 (Agilent, Japan) was used for the investigation of dielectric properties. The data were collected in the frequency range $50 – 30\times10^6$ Hz. The data were further fitted according to the Havriliak-Negami empirical model [29]:

$$\varepsilon^* = \varepsilon_\infty^{'} + \frac{\left(\varepsilon_0^{'} - \varepsilon_\infty^{'}\right)}{\left(1 + \left(i\omega \cdot t_{rel}\right)^a\right)^b} \qquad (1)$$

where ε^* stands for complex permittivity, ε'_0 and ε'_∞ are static relative permittivity and theoretical relative permittivity at infinite frequency, respectively. Their difference expresses the dielectric relaxation strength, $\Delta\varepsilon'$. Parameter ω represents angular frequency, τ_{rel} is the relaxation time, and a and b are shape parameters. Last two parameters enable to fit asymmetric relaxation peaks; the former one describing the width of the relaxation peak and the latter its asymmetry [29].

3 Results and discussion

3.1 Preparation of PpPDA

The oxidation of aniline in acidic aqueous media yields PANI. It may be proposed that a similar reaction performed with *p*-phenylenediamine would lead to a PANI-like structure (Fig. 1a). The involvement of both amine groups could produce a "polyphenazine" ladder-like polymer, which can be regarded as being composed of two entwined PANI chains (Fig. 1b). The real situation is probably more complex and can involve the branching of chains at free amino groups, various oxidation

states simulating the leucoemeraldine–emeraldine–pernigraniline transitions, possible involvement of oxygen-containing quinonoid groups, etc.

As the starting structure is not exactly known, it would be premature to speculate what happens after carbonization. For PANI, however, the production of cross-linked phenazine-containing structures has been proposed [22]. A similar structure of a nitrogen-containing carbon can probably be expected also in the present case.

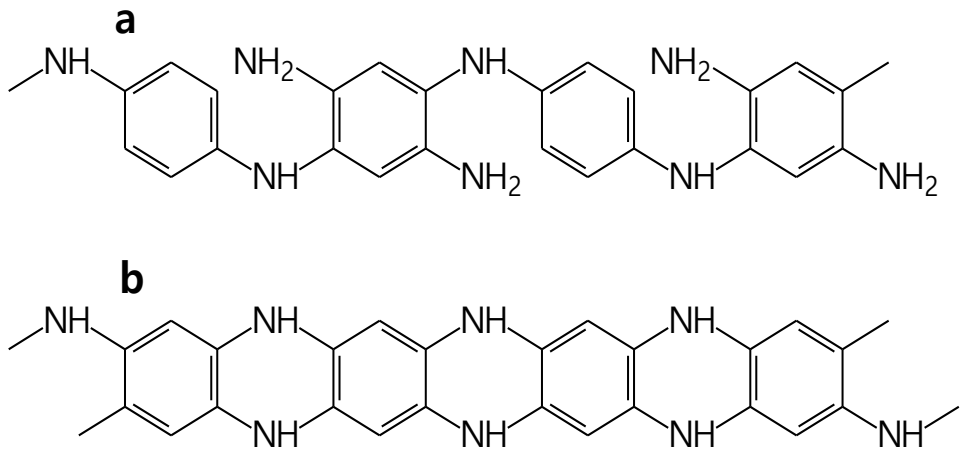

Fig. 1. Idealized structure of P*p*PDA produced by the oxidation of (a) one or (b) both amine groups in *p*-phenylenediamine.

3.2 Raman spectroscopy

To test the hypothesis concerning the molecular structure of P*p*PDA obtained with two oxidation levels, with 0.25 and 0.5 M APS, and to check if the carbonization was successful, the process was followed with Raman spectroscopy.

A Raman spectrum of P*p*PDA prepared with equimolar amount of oxidant (in Fig. 2 labeled as 1×) is similar to the spectrum of P*p*PDA observed by Sestrem et al. [30]. A shoulder at about 1647 cm^{-1} belongs to the vibrations of phenazine- and oxazine-like structures [31, 32]. The peak at 1597 cm^{-1} is attributed to the ring-stretching vibrations, that at 1520 cm^{-1} is connected with C=N stretching vibrations in quinoneiminoid or phenazine-like units [33–35]. The another one at 1455 cm^{-1}

with a shoulder at 1413 cm^{-1} belongs to the skeletal vibrations and to the oxidized phenazine-like structure [34]. Two bands located at 1320 and 1178 cm^{-1} were assigned to C–H bending on benzenoid or quinonoid ring vibrations, respectively [35]. These bands were observed for P*p*PDA but not for poly(*o*-phenylenediamine) [30]. The peak at 577 cm^{-1} is attributed to the vibrations of phenazine-like linkages [36]. Finally, weak peaks at 498, 519, 457 and 411 cm^{-1} are connected with skeletal deformations.

The spectrum of P*p*PDA prepared at doubled amount of oxidant (in Fig. 2 labeled as 2×) is not as clear as the previous spectrum and the bands are broader. The shoulder at 1647 cm^{-1} is more pronounced, the shoulder at 1413 cm^{-1} developed into a strong band. Small peaks below 500 cm^{-1} are not observed. These changes may be connected with higher ratio of phenazine-like structures (Fig. 1b) and due to the crosslinking. The bands connected with *para*-coupled chains are still present in the spectrum. The spectrum thus corresponds rather to a randomly linked and branched material than to a perfect ladder-like structure presented in Fig. 1b [37].

After heating to 200 °C (Fig. 2, 1× 200 °C and 2× 200 °C) a broad band at 1394 cm^{-1} appears for both materials. This band is connected with short oligomers of aniline, the structures potentially containing phenazine-like and benzoquinone structures [38]. This band becomes even stronger after heating to 400 °C (Fig. 2, 1× 400 °C and 2× 400 °C). After heating to 600 °C or higher temperatures (Fig. 2, 1× or 2×, 600, 650, and 800 °C), two broad bands located around 1570 and 1330 cm^{-1} are observed. These bands can be considered as G-band ("graphitic" band, stretching of any pair of sp^2 carbons) and D-band ("disorder" band, breathing of hexagonal carbon rings activated by any defect included by a heteroatom), which are defined for graphitic material [39] and proved to be applicable for a nitrogen-

containing analogue. The spectrum corresponds to the disordered nitrogen-containing graphitic material [18].

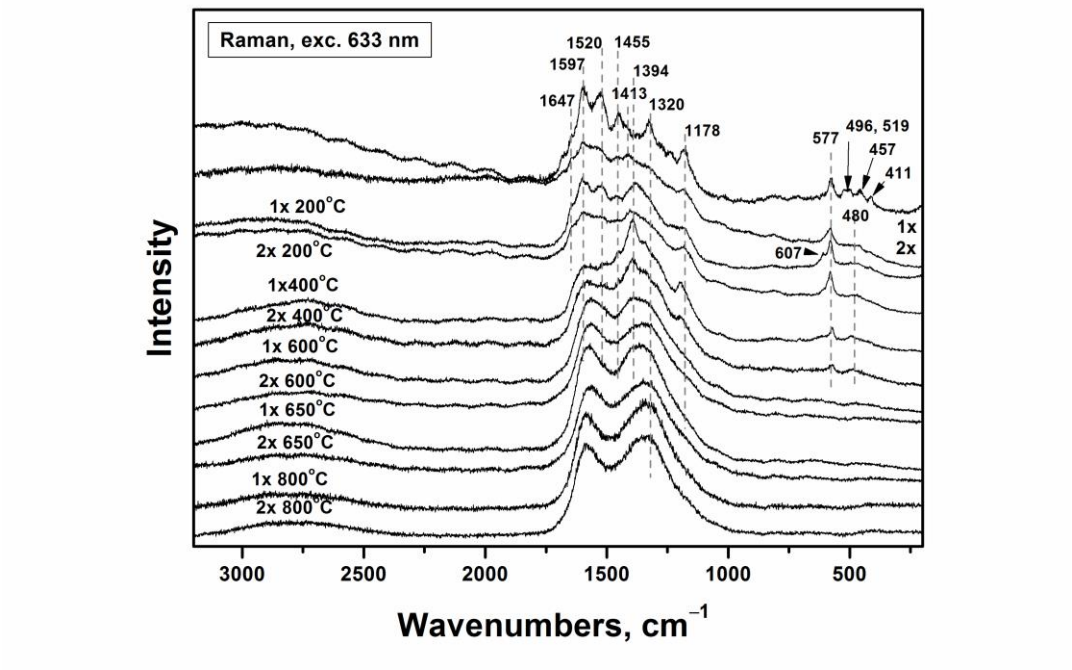

Fig. 2. Raman spectra of P*p*PDA prepared by oxidation of 0.2 M *p*-phenylenediamine with 0.25 (1×) or 0.5 M (2×) APS as prepared and after heating to various temperatures in nitrogen atmosphere.

3.3 Morphology

P*p*PDA has an irregular morphology (Fig. 3a, b), the particle size being smaller when higher oxidant concentration had been used. Its features are preserved after carbonization at 600 °C (Fig. 3c, d).

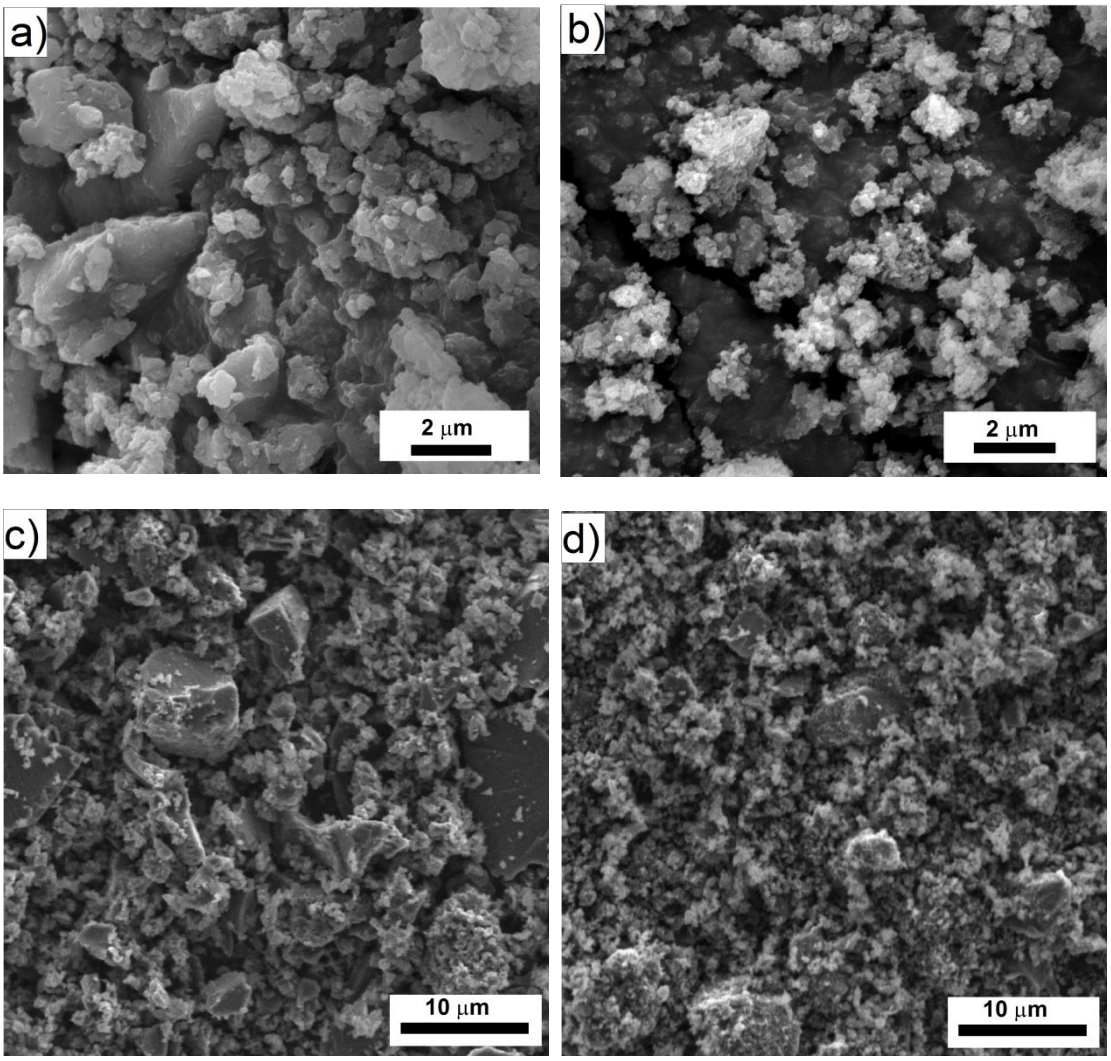

Fig. 3. Scanning electron micrographs of original samples prepared by oxidation of 0.2 M *p*-phenylenediamine with 0.25 (a) or 0.5 M (b) APS, and the same samples after carbonization at 600 °C in nitrogen atmosphere (c, d).

3.4 Analytical carbonization: Thermogravimetric analysis

The carbonization of P*p*PDA can be understood on the basis of thermogravimetric analysis, which is its analytical equivalent. As can be seen in Fig. 4, the P*p*PDA prepared at lower oxidant-to-monomer mole ratio is more stable both in nitrogen atmosphere (Fig. 4a) and in air (Fig. 4b). Carbonization in nitrogen leaves 40 – 50 wt% residue at exposure to 800 °C (Fig. 4a), while in air the samples are practically completely decomposed (Fig. 4b). However, it can be found that the modification at temperatures below 300 °C, used sometimes in the literature [18, 20, 21], leaves a sufficiently large residue similar for both environments.

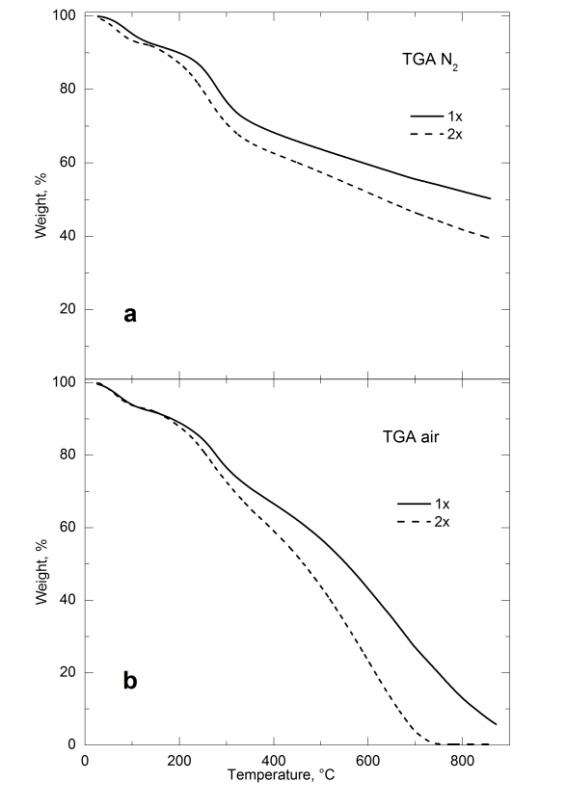

Fig. 4. Thermogravimetric analysis of P*p*PDA, prepared by oxidation of 0.2 M *p*-phenylenediamine with 0.25 (1×) or 0.5 M (2×) APS, in (a) nitrogen atmosphere and (b) in air.

3.5 Electrorheology

After carbonization of P*p*PDA at various temperatures, suspensions for ER measurements were prepared. However, particles carbonized at 650 and 800 °C were found not to be suitable for the use in ER suspensions because of their excessive conductivity that caused short circuits in the measuring device. Therefore, these materials are not discussed below. From synthesis of various types of P*p*PDA particles, those prepared with a double amount of APS showed more interesting ER responses in silicone oil suspensions and were analyzed in more detail.

For ER fluids a low field-off viscosity is one of key demands [10]. Therefore, this parameter was one of the important aspects in ER performance of the systems. Fig. 5 shows the dependence of the field-off viscosity, η_0, on the shear rate, $\dot{\gamma}$. The ER suspension of the original P*p*PDA particles, i.e. non-carbonized, exhibits the lowest field-off viscosity. With increasing carbonization temperature the field-off viscosity significantly rises. Especially at low shear rates the viscosity of investigated ER suspensions differs approximately by one order of magnitude.

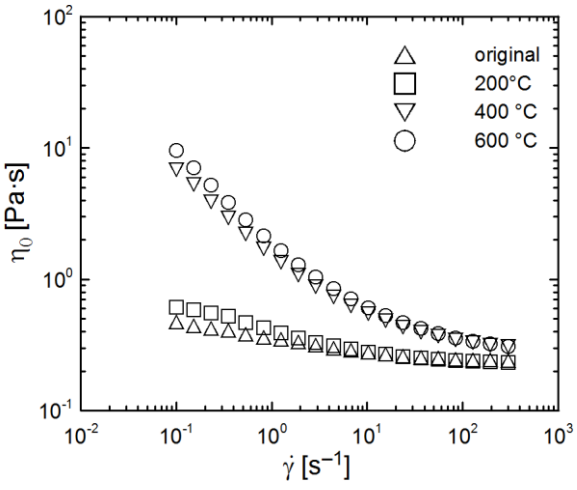

Fig. 5. Dependence of the field-off viscosity, η_0, on the shear rate, $\dot{\gamma}$, for 10 wt% ER fluids based on P*p*PDA particles carbonized under various temperatures in nitrogen atmosphere.

The generation of internal structures can be confirmed by the examination of flow properties of ER fluids in the presence of external electric field. Fig. 6a and Fig. 6b show rheological properties of ER fluids in the absence and in the presence of electric field of 2 kV mm^{-1}, respectively. A substantial increase in the shear stress reflecting the appearance of chain-like structures upon the application of electric field can be observed. This is caused by the formation of stiff internal structures within the system whose rupture occurs only above a yield stress, τ_0 [8].

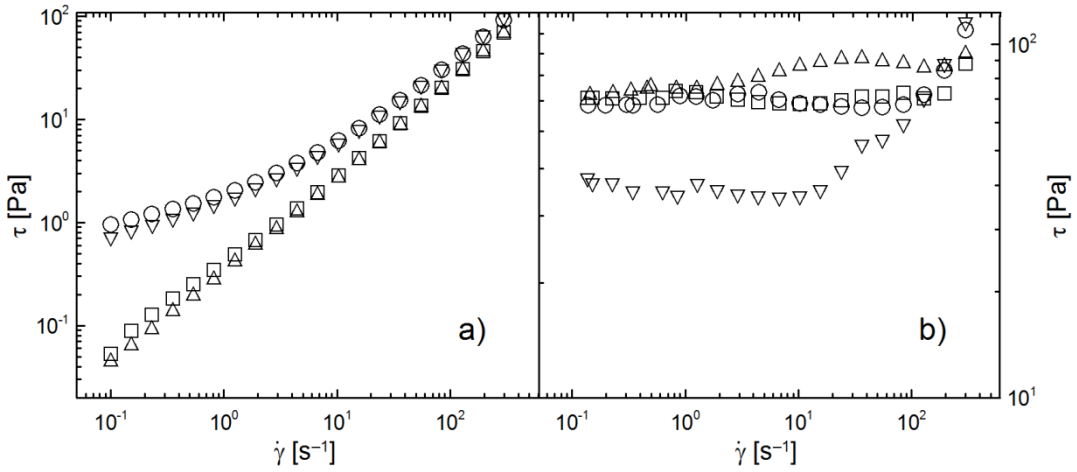

Fig. 6. The double-logarithmic plot of shear stress, τ, in the absence (a) and in the presence of electric field strength of 2 kV mm^{-1} (b) on shear rate, $\dot{\gamma}$. The meaning of symbols is the same as in Fig. 5.

The highest yield stress is observed for the ER suspension based on the original P*p*PDA particles. However, there is no substantial difference in the ER effect

between these particles and those carbonized at 200 and 600 °C, while particles carbonized at 400 °C show the lowest response on the applied electric field. This can be partially explained as the consequence of conductivity of these particles. Rozlívková et al. [24] worked with carbonized granular PANI and their measurements revealed that electric conductivity increases for particles carbonized at 600 °C. These particles had the conductivity 1.2×10^{-8} S cm^{-1}, while original PANI base conductivity was 1.7×10^{-10} S cm^{-1}. Further, the particles exposed to 200 °C or 400 °C had a similar conductivity as the original PANI base or even lower by one order of magnitude, respectively. Thus, the low conductivity of particles carbonized at 400 °C could partially clarify the low ER effect. This can elucidate the ER performance of investigated particles in electric field, since P*p*PDA is a derivate of PANI, and thus similar behavior can be expected. However, too high conductivity of particles can lead to shortcuts of the device in practical applications, as already mentioned.

The ER efficiency, *e*, is another important factor in ER systems as it evaluates the behavior change of the system in the absence and in the presence of external electric field. It can be calculated according to Eq. (2):

$$e = \frac{(\eta_E - \eta_0)}{\eta_0} \tag{2}$$

where η_E is viscosity in the presence of the electric field and η_0 is field-off viscosity. Fig. 7 shows the dependence of ER efficiency, *e*, on shear rate, $\dot{\gamma}$. As can be seen, the highest ER efficiency was achieved for suspensions based on original P*p*PDA particles. However, the suspension based on particles carbonized at 200 °C exhibited only slightly lower ER efficiency. A substantially lower ER response can be observed for suspensions based on particles carbonized at 400 °C and 600 °C, which

is caused by the low ER effect and the high field-off viscosity. At high shear rates, the differences in various ER fluids are reduced due to the dominance of hydrodynamic forces.

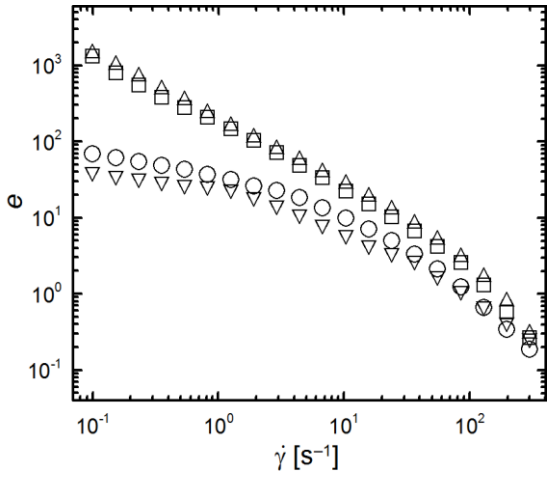

Fig. 7. Dependence of ER efficiency, *e*, (calculated from viscosity at 0 and 2 kV mm^{-1}) for ER fluids based on P*p*PDA particles (carbonized under different temperatures in nitrogen atmosphere) on shear rate, $\dot{\gamma}$. The meaning of symbols is the same as in Fig. 5.

Even better description of these smart systems, in connection to applications, can be obtained from oscillatory tests represented by dynamic loadings. These tests give a picture of viscoelastic behavior of the materials. Fig. 8 shows the dependence of storage and viscous moduli on angular frequency in the absence (a) and in the presence (b) of external electric field. From the Fig. 8a it is evident that the storage (elastic) modulus, G', and the loss (viscous) modulus, G'', exhibit nearly the same values. Thus, there is no dominance of any modulus. However, after the application of the electric field (Fig. 8b) G' increases more significantly than G'' and its

dominance is apparent. This is connected with transition from the liquid to solid-like state caused by the formation of organized structure within the ER fluid. It can be seen that the highest storage modulus was achieved for original P*p*PDA particles.

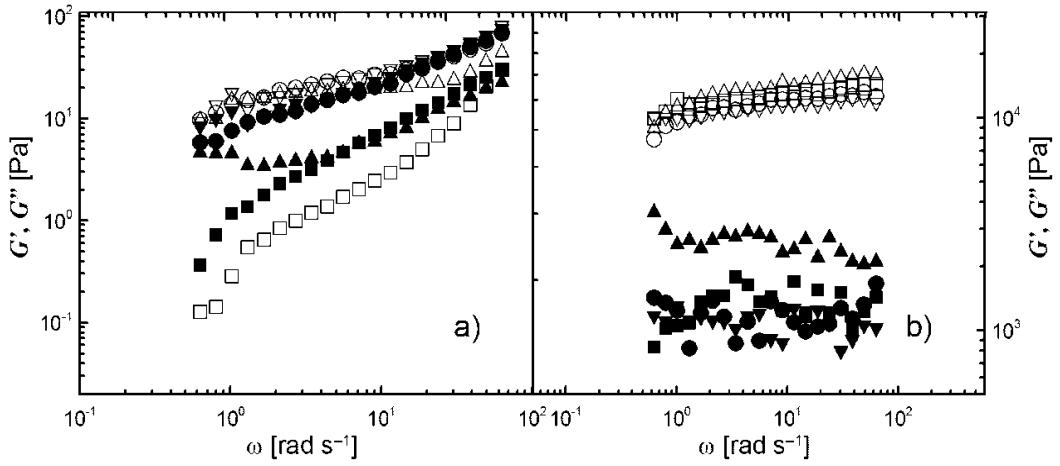

Fig. 8. Dependence of storage modulus (open symbols), *G′*, and viscous modulus (solid symbols), *G″*, on angular frequency, *ω*, in the absence (a) and in the presence of electric field strength of 2 kV mm^{-1} (b). The meaning of symbols is the same as in Fig. 5.

3.6. Dielectric properties

It is assumed that interfacial polarization of particles plays a dominant role in the ER performance. It was proposed [5] that a good ER fluid should have its dielectric relaxation time between $10^2 – 10^5$ Hz and the dielectric relaxation strength should be large. Thus, dielectric properties were analysed and Eq. (1) was applied for data evaluation. The obtained results are presented in Tab. 1. As can be seen, suspensions based on original particles and particles carbonized at 200 °C and 600 °C possess short relaxation times, which correspond well to the ER response of these suspensions to external electric field. The suspension based on particles carbonized at 600 °C exhibits the highest dielectric relaxation strength; its response to the

electric field, however, is similar to the suspensions based on original particles and particles carbonized at 200 °C.

Table 1 – Dielectric parameters obtained from Havriliak-Negami model.

Parameter	Carbonization temperature [°C]			
	Original	200	400	600
ε'_0	4.06	4.07	4.35	4.63
ε'_∞	3.10	3.05	3.00	2.03
$\Delta\varepsilon'$	0.96	1.02	1.35	1.60
τ_{rel} [s]	2.68×10^{-6}	8.54×10^{-5}	3.16×10^{-3}	5.50×10^{-6}
a	0.98	0.53	0.66	0.99
b	0.59	0.62	0.68	0.62

This can be seen also in Fig. 9, which shows the dependence of real, ε', and imaginary, ε'', part of relative permittivity on the frequency, f. The relaxation time of the suspension based on the particles carbonized at 400 °C is 4.02×10^{-3} s, which means that it does not fulfill the above mentioned criterion for sufficient ER performance.

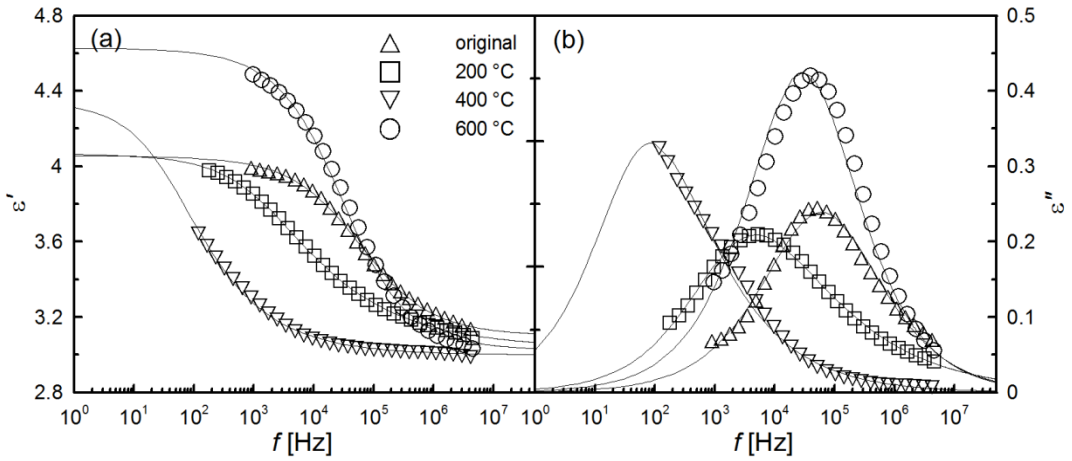

Fig. 9. Dielectric spectra of relative permittivity (a) and dielectric loss factor (b) for ER fluids based on original particles, and particles carbonized at 200 °C, 400 °Cand 600 °C.

4 Conclusion

Poly(*p*-phenylenediamine) particles were carbonized at different temperatures in inert nitrogen atmosphere. Carbonization was followed by thermogravimetric analysis, which showed the higher thermal stability of P*p*PDA particles prepared by a lower amount of oxidant. The conversion to the disordered nitrogen-containing carbon with increasing carbonization temperature was observed. Particles were subsequently used for the preparation of ER fluids which exhibit a distinct ER performance. With increasing electric field strength the ER response was higher. The highest ER efficiency was observed for original, i.e. non-carbonized sample. The ER efficiency decreased as the carbonization temperature increased, i.e. carbonization of P*p*PDA particles had a negative effect on ER behavior.

Acknowledgments

The authors wish to thank the Czech Grant Agency (202/09/1626) for the financial support. This research was also carried out with support of the Operational Programme Research and Development for Innovations co-funded by the European Regional Development Fund (ERDF) and national budget of the Czech Republic, within the framework of the Centre of Polymer Systems project (CZ.1.05/2.1.00/03.0111).

References

[1] Quadrat O, Stejskal J. Polyaniline in electrorheology. J Ind Eng Chem 2006; 12: 352–361.

[2] Yin JB, Zhao XP. Electrorheology of nanofiber suspensions. Nanoscale Res Lett 2011; 6: 1–17.

[3] Plocharski J, Drabik H, Wyciślik H, Ciach T. Electrorheological properties of polyphenylene suspensions. Synth Met 1997; 88: 139–145.

[4] Sung JH, Cho MS, Choi HJ, Jhon MS. Electrorheology of semiconducting polymers. J Ind Eng Chem 2004; 10: 1217–1229.

[5] Hao T. Electrorheological suspensions. Adv Colloid Interface Sci 2002; 97: 1–35.

[6] Davis LC. Time-dependent and nonlinear effects in electrorheological fluids. J Appl Phys 1997; 81: 1985–1991.

[7] Trlica J, Saha P, Quadrat O, Stejskal J. Electrical and electrorheological behavior of poly(aniline-*co*-1,4-phenylendiamine) suspensions. Eur Polym J 2000; 36: 2313–2319.

[8] Pavlinek V, Saha P, Kitano T, Stejskal J, Quadrat O. The effect of polyaniline layer deposited on silica particles on electrorheological and dielectric properties of their silicone–oil suspensions. Physica A 2005; 353: 21–28.

[9] Sedlacik M, Mrlik M, Pavlinek V, Saha P. Electrorheological properties of suspensions of hollow globular titanium oxide/pyrrole particles. Colloid Polym Sci 2012; 290: 41–48.

[10] Yin J, Shui Y, Chang R, Zhao X. Graphene-supported carbonaceous dielectric sheets and their electrorheology. Carbon 2012; 50: 5247–5255.

[11] Kim DH, Kim YD. Electrorheological properties of polypyrrole and its composite ER fluids. J Ind Eng Chem 2007; 13: 879–894.

[12] Choi HJ, Jhon MS. Electrorheology of polymers and nanocomposites. Soft Matter 2009; 5: 1562–1567.

[13] Sim IS, Kim JW, Choi HJ, Kim ChA, Jhon MS. Preparation and electrorheological characteristics of poly(*p*-phenylene)-based suspensions. Chem Mater 2001; 13: 1243–1247.

[14] Trlica J, Saha P, Quadrat O and Stejskal J. Electrorheological activity of polyphenylenediamine suspensions in silicone oil. Physica A 2000; 283: 337–348.

[15] Choi HJ, Cho MS, To K. Electrorheological and dielectric characteristics of semiconductive polyaniline-silicone oil suspensions. Physica A 1998; 254: 272–279.

[16] Choi HJ, Cho MS, Jhon MS. Electrorheological properties of poly(acene quinone) radical suspensions. Polym Adv Tech 1997; 8: 697–700.

[17] Fang FF, Liu YD, Lee IS, Choi HJ. Well controlled core/shell type polymeric microspheres coated with conducting polyaniline: fabrication and electrorheology. RSC Adv 2011; 1: 1026–1032.

[18] Xia X, Yin JB, Qiang PF, Zhao XP. Electrorheological properties of thermo-oxidative polypyrrole nanofibers. Polymer 2011; 52: 786–792.

[19] Yin JB, Xia X, Xiang LQ, Zhao XP. Temperature effect of electrorheological fluids based on polyaniline derived carbonaceous nanotubes. Smart Mater Struct 2011; 20: 015002 (1–8).

[20] Yin JB, Xia X, Zhao XP. Polym Degrad Stab 2012; 97: 2356–2363.

[21] Chen YZ, Wang BP, Dong SJ, Wang YP, Liu YN. Rectangular microscale carbon tubes with protuberant wall for high-rate electrochemical capacitors. Electrochim Acta 2012; 80: 34–40.

[22] Trchová M, Konyushenko EN, Stejskal J, Kovářová J, Ćirić-Marjanović G. The conversion of polyaniline nanotubes to nitrogen-containing carbon nanotubes and their comparison with multi-walled carbon nanotubes. Polym Degrad Stab 2009; 94: 929–938.

[23] Bae JW, Jang JS. Fabrication of carbon nanotubes from conducting polymer precursor as field emitter. J Ind Eng Chem 2012; 18: 1921–1924.

[24] Rozlívková Z, Trchová M, Exnerová M, Stejskal J. The carbonization of granular polyaniline to produce nitrogen-containing carbon. Synth Met 2011; 161: 1122–1129.

[25] Yin J, Xia X, Xiang L, Zhao X. Conductivity and polarization of carbonaceous nanotubes derived from polyaniline nanotubes and their electrorheology when dispersed in silicone oil. Carbon 2010; 48: 2958–2967.

[26] Gavrilov N, Pašti IA, Mitrić M, Travas-Sejdić J, Ćirić-Marjanović G, Mentus SV. Electrocatalysis of oxygen reduction reaction on polyaniline-derived nitrogen-doped carbon nanoparticle surfaces in alkaline media. J Power Sources 2012; 220: 306–316.

[27] Yuan DS, Zhou TX, Zhou SL, Zou WJ, Mo SS, Xia NN. Nitrogen-enriched carbon nanowires from the direct carbonization of polyaniline nanowires and its electrochemical properties. Electrochem Commun 2011; 13: 242–246.

[28] Yuan DS, Yuan XL, Zhou SL, Zou WJ, Zhou TX. N-Doped carbon nanorods as ultrasensitive electrochemical sensors for the determination of dopamine. RSC Adv 2012; 2: 8157–8163.

[29] Havriliak S, Negami S. A complex plane analysis of α-dispersions in some polymer systems. J Polym Sci 1966; 14: 99–117.

[30] Sestrem RH, Ferreira DC, Landers R; Temperini MLA, do Nascimento GM. Structure of chemically prepared poly-(para)phenylendiamine) investigated by spectroscopic techniques. Polymer 2009; 50: 6043–6048.

[31] Brolo AG, Sanderson AC. Surface-enhanced Raman scattering (SERS) from a silver electrode modified with oxazine 720. Can J Chem 2004; 82: 1474–1480.

[32] Do Nascimento GM, Silva CHB, Temperini MLA. Spectroscopic characterization of the structural changes of polyaniline nanofibers after heating. Polym Degrad Stab 2008; 93: 291–297.

[33] Quillard S, Louarn G, Lefrant S, MacDiarmid AG. Vibrational analysis of polyaniline – a comparative study of leucoemeraldine, emeraldine, and pernigraniline bases. Phys Rev B 1994; 50: 12496–12508.

[34] Malinauskas A, Bron M, Holze R. Electrochemical and Raman spectroscopic studies of electrosynthesized copolymers and bilayer structures of polyaniline and poly(*o*-phenylenediamine). Synth Met 1998; 92: 127–137.

[35] Boyer MI, Quillard S, Rebourt E, Louarn G, Buisson JP, Monkman A, et al. Vibrational analysis of polyaniline: A model compound approach. J Phys Chem B 1998; 102: 7382–7392.

[36] Do Nascimento GM, Silva CHB, Temperini MLA. Electronic structure and doping behaviour of PANI-NSA nanofibers investigated by resonance Raman spectroscopy. Macromol Rapid Commun 2006; 27: 255–259.

[37] Baibarac M, Baltog I, Scocioreanu M, Ballesteros B, Mevellec JY, Lefrant S. One-dimensional composites based on single walled carbon nanotubes and poly(*o*-phenylenediamine). Synth Met 2011; 161: 2344–2354.

[38] Surwade SP, Dua V, Manohar N, Manohar SK, Beck E, Ferraris JP. Oligoaniline intermediates in the aniline–peroxydisulfate system. Synth Met 2009; 159: 445–455.

[39] Dresselhaus MS, Jorio A, Hofman M, Dresselhaus G, Saito R. Perspectives on carbon nanotubes and graphene Raman spectroscopy. Nano Lett 2010; 10: 751–758.

Figure captions

Fig. 1. Idealized structure of P*p*PDA produced by the oxidation of (a) one or (b) both amine groups in *p*-phenylenediamine.

Fig. 2. Raman spectra of P*p*PDA prepared by oxidation of 0.2 M *p*-phenylenediamine with 0.25 (1×) or 0.5 M (2×) APS as prepared and after heating to various temperatures in nitrogen atmosphere.

Fig. 3. Scanning electron micrographs of original samples prepared by oxidation of 0.2 M *p*-phenylenediamine with 0.25 (a) or 0.5 M (b) APS, and the same samples after carbonization at 600 °C in nitrogen atmosphere (c, d).

Fig. 4. Thermogravimetric analysis of P*p*PDA, prepared by oxidation of 0.2 M *p*-phenylenediamine with 0.25 (1×) or 0.5 M (2×) APS, in (a) nitrogen atmosphere and (b) in air.

Fig. 5. Dependence of the field-off viscosity, η_0, on the shear rate, $\dot{\gamma}$, for 10 wt% ER fluids based on P*p*PDA particles carbonized under various temperatures in nitrogen atmosphere.

Fig. 6. The double-logarithmic plot of shear stress, τ, in the absence (a) and in the presence of electric field strength of 2 kV mm^{-1} (b) on shear rate, $\dot{\gamma}$. The meaning of symbols is the same as in Fig. 5.

Fig. 7. Dependence of ER efficiency, *e*, (calculated from viscosity at 0 and 2 kV mm^{-1}) for ER fluids based on P*p*PDA particles (carbonized under

different temperatures in nitrogen atmosphere) on shear rate, $\dot{\gamma}$. The meaning of symbols is the same as in Fig. 5.

Fig. 8. Dependence of storage modulus (open symbols), *G′*, and viscous modulus (solid symbols), *G″*, on angular frequency, *ω*, in the absence (a) and in the presence of electric field strength of 2 kV mm^{-1} (b). The meaning of symbols is the same as in Fig. 5.

Fig. 9. Dielectric spectra of relative permittivity (a) and dielectric loss factor (b) for ER fluids based on original particles, and particles carbonized at 200 °C, 400 °Cand 600 °C.

Table caption

Table 1 – Dielectric parameters obtained from Havriliak-Negami model.